Computers and Mathematics with Applications 64 (2012) 2775–2786

Contents lists available at SciVerse ScienceDirect

Computers and Mathematics with Applications

journal homepage: www.elsevier.com/locate/camwa

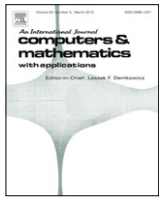

Modelling and parameter re-identification of nanoindentation of soft polymers taking into account effects of surface roughness

Zhaoyu Chen *, Stefan Diebels **

Chair of Applied Mechanics, Saarland University, PO Box 151150, 66041, Saarbrücken, Germany

ARTICLE INFO

Article history:
Received 1 February 2012
Received in revised form 3 April 2012
Accepted 12 April 2012

Keywords:
Numerical modelling of nanoindentation
Soft polymer
Surface roughness
Parameter identification

ABSTRACT

In this paper the characterisation of polymers by nanoindentation is investigated numerically by the use of the inverse method. Effects of the surface roughness are explicitly considered. The boundary value problems of the nanoindentation of two polymers, PDMS and silicone rubber, are modelled with the FE code ABAQUS®. The model parameters are re-identified by using an evolution strategy based on the concept of the numerical optimisation. The surface roughness effects are investigated numerically by explicitly taking into account the roughness profile in the model. At first the surface roughness is chosen to have a simple representation considering only one-level of asperities described by a sine function. The influence of the surface roughness is quantified as a function of the sine parameters as well as of the indentation parameters. Moreover, it is verified that the real surface topography can be characterised by using multi-level or simple one-level of protuberance-on-protuberance sinusoidal roughness strain-energy function. profiles. The effects of the surface roughness are investigated with respect to the force–displacement data and the identified model parameters. These numerical results are expected to offer a deep insight into the influence of the real surface roughness at the results of indentation tests.

1. Introduction

Over the last decades, the nanoindentation testing technique has continuously been improved. Now it is widely applied in metallic and ceramic engineering materials to determine the mechanical properties such as hardness and modulus. Since this technique is able to measure the properties of extremely small volumes with sub-μm and with sub-μN resolution, it also became one of the primary testing techniques for the mechanical characterisation of polymeric materials and biological tissues. The analysis of individual indentation tests by using the conventionally applied Oliver and Pharr method (abbreviated as O&P method) [1,2] is limited with regard to capture the hyperelastic and the rate-dependent properties of polymers and some metals. Therefore, numerical approaches in combination with the experimental testing, i.e. the finite element simulations and numerical optimisation have been used and evolved [3–13]. In this method, the difference between the experimental data and the numerical prediction is minimised with respect to the material model parameters by using numerical optimisation. The parameters are identified as the optimised solution.

Nanoindentation has the considerable advantage to measure the local properties of small volume materials from the continuously sensed force–displacement curve. However, it includes various error contributions, e.g. friction, adhesion, surface roughness and indentation process associated factors. These contributions generate the systematic errors between

* Corresponding author. Tel.: +49 0 681 302x2169.
** Corresponding author. Tel.: +49 0 681 302x2887.
E-mail addresses: zh.chen@mx.uni-saarland.de (Z. Chen), s.diebels@mx.uni-saarland.de (S. Diebels).

0898-1221/$ – see front matter © 2012 Elsevier Ltd. All rights reserved.
doi:10.1016/j.camwa.2012.04.010

the numerical model and the experiments, and this often leads to large errors in the parameter identification [9,14–16]. Therefore, basic investigations and the certain knowledge about the influence of these factors are indispensable to characterise the materials accurately from nanoindentation based on the inverse method.

It is recognised by the use of the experimental and the numerical approaches that the surface roughness has a significant influence on the force–displacement data at a small or a moderate indentation depth, which is comparable to the height of the surface asperities [17–29]. It is known by the experimental investigation that the surface roughness impacts the Young's modulus and the hardness measurements [17,18,21,24]. The surface roughness can considerably disturb the indentation curves [22], and may, at least, be one of the main reasons for the indentation size effect [23]. The criteria to remove the surface roughness effects are found by experiments for some special materials. Miller et al. [28] found that it is possible to get a unique set of material properties if the average indentation depth is 5 times greater than the RMS roughness. For cancellous bone Donnelly et al. [29] pointed out that the variability in material properties increases substantially if the ratio of indentation depth to surface roughness decreases below 3:1. The surface roughness effects are difficult to control in an experiment, and moreover the measuring results are not easily to interpret. Nevertheless, the numerical simulation tools may help to understand the physics involved in this complex experiment. Therefore, FE simulations are widely used to interpret the experimental results if surface roughness effects are included [26,27,30,20]. The results in [26,27,30] have shown that an increasing roughness causes an increasing scatter of the data, but the mean value of a sufficiently large number of indents can still give a good approximation of the Young's modulus. Jiang et al. [20] pointed out that in order to rule out the influence of the surface morphology, the indentation depth should be much greater than the characteristic size of the surface roughness. Moreover, an indenter with a sufficiently large diameter could also be a good choice. A numerical study was conducted in [19] to understand the coupled influence of friction and surface roughness in the nanoindentation of pure nickel. Results have shown a strong interaction between these two contributions of surface effects, and their cumulative effects leads to significant variations in the force–displacement curves. The surface roughness of the bulk sample can be altered by various mechanical or electrochemical methods of polishing. However, an excessive polishing could influence the mechanical properties of soft and thin polymer films. Therefore, in practical experiments, the surface roughness of thin films can reach an average height of asperities about 30–60 nm [21,31,32]. Because of that, the surface roughness is comparable to the imposed indentation depth limited by the thin layer's thickness and the influence of the substrate. In this case, some of the criteria documented in the literature cannot be used longer. A quantified evaluation of the surface roughness effect is still required. Furthermore, it is essential to decrease the errors between the experimental settings and the numerical simulations if the inverse method is used. For this reason, more attention is paid on the numerical model of the realistic surface roughness profile. The surface roughness for the finite element models is taken from AFM data of sputter-deposited CrN within 2D and 3D in [26,27]. Pre-existing straight grooves defects are introduced on the film surface in 2D FE models in [20]. Berke et al. [19] describes the roughness with a protuberance-on-protuberance profile approximated by a sine function using axisymmetric 2D FE models.

In this present article, the behaviour of two hyperelastic soft polymers under nanoindentation is investigated numerically taking into account the effects of the surface roughness. The characterisation of the materials' properties is performed based on parameter re-identification procedure by using the inverse method. In this procedure, the virtual experimental data, which are obtained from numerical simulations with the chosen parameters, replace the real experimental measurements. In this sense, the finite element code ABAQUS® is used as a virtual laboratory. The parameter re-identification concept was used in [9,33] to validate the gradient-based material parameter identification routine. The surface roughness effects are investigated numerically based on the approach, which is mainly influenced by the work of Kumar et al. [21] and Berke et al. [19]. The surface roughness is chosen to have a simple representation considering a one-level roughness profile described in a first step by a sine function. The influence of the surface roughness is quantified phenomenological as a function of the sine curve parameters as well as of the indentation parameters. Moreover, it is verified that a real surface topography can be characterised by using a multi-level or a simple one-level of protuberance-on-protuberance sinusoidal profiles. The effects of this surface roughness are investigated with respect to the identified model parameters. The whole force–displacement curve is taken into account. The results are expected to offer a deep insight into the effects of the real surface roughness by a numerical modelling of nanoindentation.

2. FEM simulation of nanoindentation

2.1. Hyperelastic material model

In the present work we consider the nanoindentation of two nearly incompressible soft polymers by numerical simulation: polydimethylsiloxane (PDMS) 1:10 used in [34] and silicone rubber ELASTOSIL® RT 265 used in [35]. Both of the two polymers were assumed to be isotropic hyperelastic materials under isothermal conditions. Firstly in the framework of finite strain continuum mechanics, constitutive models of a nearly incompressible hyperelastic material will be recalled.

The existence of the Helmholtz free-energy function Ψ is postulated for a so-called hyperelastic material. Concerning the isotropic material under isothermal conditions, $\Psi = \Psi(\mathbf{F})$ is solely a function of the deformation gradient $\mathbf{F}$ or a strain tensor, respectively. So the Helmholtz free-energy function is referred to the strain-energy function. The general format of the constitutive equation can be derived from the second law of thermodynamics in the form of the Clausius–Planck

inequality

$$\mathcal{D}_{int} = \mathbf{P} : \dot{\mathbf{F}} - \dot{\Psi} = \left(\mathbf{P} - \frac{\partial \Psi(\mathbf{F})}{\partial \mathbf{F}} \right) : \dot{\mathbf{F}} \geq \mathbf{0}, \tag{1}$$

where $\mathcal{D}_{int}$ and $\mathbf{P}$ are the internal dissipation and the 1^{st} Piola–Kirchhoff stress tensor, respectively. Only if $\mathbf{F}$ is chosen as a process variable influencing the free energy, $\mathbf{F}$ and hence $\dot{\mathbf{F}}$ can be chosen arbitrarily. Therefore, the expression in parentheses must be zero and the constitutive equation associated with $\mathbf{P}$ can be expressed as

$$\mathbf{P} = \frac{\partial \Psi(\mathbf{F})}{\partial \mathbf{F}}. \tag{2}$$

With the relations $\overline{\mathbf{T}} = \mathbf{F}^{-1}\mathbf{P}$ and $\mathbf{T} = J^{-1}\mathbf{F}\overline{\mathbf{T}}\mathbf{F}^{T}$, the 2nd Piola–Kirchhoff stress tensor $\overline{\mathbf{T}}$ and the Cauchy stress tensor $\mathbf{T}$ can be derived (details see e.g. [36, Chapter 6]). Due to the assumption that the strain-energy $\Psi(\mathbf{F})$ generated by the motion $\mathbf{x} = \widetilde{\boldsymbol{\chi}}(\mathbf{X}, t)$ is objective as well as the fact that $\Psi(\mathbf{F})$ remains unchanged if a rigid-body motion is superimposed on the isotropic hyperelastic material, $\Psi(\mathbf{F})$ can also be described as

$$\Psi(\mathbf{F}) = \Psi(\mathbf{C}) = \Psi(\mathbf{B}) \tag{3}$$

with the right Cauchy–Green deformation tensor $\mathbf{C} = \mathbf{F}^{T} \cdot \mathbf{F}$ and the left Cauchy–Green deformation tensor $\mathbf{B} = \mathbf{F} \cdot \mathbf{F}^{T}$.

Since compressible materials behave quite differently in the bulk and the shear deformation, it is most useful to split the deformation locally into a so-called volumetric part and an isochoric part. In particular, we consider the multiplicative decomposition of $\mathbf{F}$, $\mathbf{C}$ and $\mathbf{B}$ into volumetric parts and isochoric parts

$$\mathbf{F} = (J^{1/3}\mathbf{I})\bar{\mathbf{F}} = (J^{1/3})\bar{\mathbf{F}}, \qquad \mathbf{C} = (J^{2/3}\mathbf{I})\bar{\mathbf{C}} = (J^{2/3})\bar{\mathbf{C}}, \qquad \mathbf{B} = (J^{2/3}\mathbf{I})\bar{\mathbf{B}} = (J^{2/3})\bar{\mathbf{B}}. \tag{4}$$

The terms $J^{1/3}\mathbf{I}$ and $J^{2/3}\mathbf{I}$ are related to volume-changing deformation, while $\bar{\mathbf{F}}$, $\bar{\mathbf{C}} = \bar{\mathbf{F}}^{T}\bar{\mathbf{F}}$ and $\bar{\mathbf{B}} = \bar{\mathbf{F}}\bar{\mathbf{F}}^{T}$ are associated with volume-preserving deformations, with the rules

$$\det \bar{\mathbf{F}} = 1, \qquad \det \bar{\mathbf{C}} = \det \bar{\mathbf{B}} = (\det \bar{\mathbf{F}})^2 = 1. \tag{5}$$

Based on the kinematic assumption above, the extension to the nearly incompressible hyperelastic behaviour is by additively decomposing the Helmholtz free-energy function Ψ into the volumetric elastic part Ψ_{vol} and the isochoric elastic part Ψ_{iso}. For isotropic materials, it is further assumed that Ψ is expressed in terms of the principle invariants of the modified Cauchy–Green tensors $\bar{\mathbf{C}}$ or $\bar{\mathbf{B}}$.

$$\Psi = \Psi_{\text{vol}}(J) + \Psi_{\text{iso}}[\bar{I}_1(\bar{\mathbf{C}}), \bar{I}_2(\bar{\mathbf{C}})] = \Psi_{\text{vol}}(J) + \Psi_{\text{iso}}[\bar{I}_1(\bar{\mathbf{B}}), \bar{I}_2(\bar{\mathbf{B}})] \tag{6}$$

The strain invariants $\bar{I}_a (a = 1, 2, 3)$ are the three modified principle invariants of $\bar{\mathbf{C}}$ and $\bar{\mathbf{B}}$, i.e.

$$\bar{I}_1 = \text{tr}\bar{\mathbf{C}} = \text{tr}\bar{\mathbf{B}}, \tag{7}$$

$$\bar{I}_2 = \frac{1}{2}\left[(\text{tr}\bar{\mathbf{C}})^2 - \text{tr}(\bar{\mathbf{C}}^2)\right] = \frac{1}{2}\left[(\text{tr}\bar{\mathbf{B}})^2 - \text{tr}(\bar{\mathbf{B}}^2)\right], \tag{8}$$

$$\bar{I}_3 = \det \bar{\mathbf{C}} = \det \bar{\mathbf{B}} = 1, \tag{9}$$

with the relationships to the principle invariants

$$\bar{I}_1 = J^{-2/3} I_1, \qquad \bar{I}_2 = J^{-4/3} I_2, \qquad \bar{I}_3 = 1. \tag{10}$$

Finally, we formulate the constitutive equation of $\overline{\mathbf{T}}$ in terms of the Jacobian J and the modified invariants $\bar{I}_1, \bar{I}_2$ (details see e.g. [36, Chapter 6])

$$\overline{\mathbf{T}} = 2\frac{\partial \Psi(\mathbf{C})}{\partial \mathbf{C}} = \overline{\mathbf{T}}_{\text{vol}} + \overline{\mathbf{T}}_{\text{iso}} \tag{11}$$

$$= J\frac{\partial \Psi_{\text{vol}}(J)}{\partial J}\mathbf{C}^{-1} + 2\frac{\partial \Psi_{\text{iso}}(\bar{I}_1, \bar{I}_2)}{\partial \bar{I}_1} : \frac{\partial \bar{I}_1}{\partial \mathbf{C}} + 2\frac{\partial \Psi_{\text{iso}}(\bar{I}_1, \bar{I}_2)}{\partial \bar{I}_2} : \frac{\partial \bar{I}_2}{\partial \mathbf{C}}. \tag{12}$$

In the framework of finite strain continuum mechanics, such formulations became popular where an additive split of the strain-energy function into isochoric parts and volumetric parts is used [37]. This type of formulation is very often used if large elastic deformations of rubber or rubber-like materials are concerned, because of the advantages in the numerical treatment of either incompressible or nearly incompressible properties. However, this formulation may lead to non-physical results if it is used without restriction to nearly incompressible materials with large volumetric deformation [37–39]. In the present study, it is reasonable to use this formulation because the investigated PDMS and silicone rubber are nearly incompressible.

Table 1
Chosen material models and parameters of the indented polymers.

Materials	Chosen models	Parameters			Shear modulus
PDMS	Neo-Hookean	C_{10} 0.662 MPa	D_1 0.255 MPa		μ_0 1.324 MPa
Silicone Rubber	Mooney–Rivlin	C_{10} 0.111 MPa	C_{01} 0.039 MPa	D_1 0.001 MPa	μ_0 0.300 MPa

There are numerous specific forms of strain-energy functions to describe the hyperelastic properties, whereas according to [34,35], the considered PDMS 1:10 and the silicone rubber can be modelled by a neo-Hookean model and a Mooney–Rivlin model [40] respectively:

$$\Psi_{\mathrm{NH}} = \Psi_{\mathrm{iso}}(\bar{I}_1) + \Psi_{\mathrm{vol}}(J) = C_{10}\,(\bar{I}_1 - 3) + \frac{1}{D_1}[(J-1)^2 + (\ln J)^2]/2, \tag{13}$$

$$\Psi_{\mathrm{MR}} = \Psi_{\mathrm{iso}}(\bar{I}_1, \bar{I}_2) + \Psi_{\mathrm{vol}}(J) \tag{14}$$

$$= C_{10}\,(\bar{I}_1 - 3) + C_{01}\,(\bar{I}_2 - 3) + \frac{1}{D_1}[(J-1)^2 + (\ln J)^2]/2. \tag{15}$$

The strain-energy function has to satisfy some physical limit conditions [41]. If the continuum is compressed to a single point, i.e. $J \to +0$, the strain energy tends to plus infinity and the volumetric stress towards to minus infinity. In the limit case if the continuum is stretched infinitely, one can obtain a plus infinite strain energy as well as a plus infinite volumetric stress. In the strainless initial state, i.e. $\bar{I}_a \to 1$ and $J \to 1$, it is a stress-free condition and no strain energy is stored. The initial shear modulus μ_0 and the initial compression modulus K_0 are related to the coefficients in the following way:

$$\mu_0 = 2\,\frac{\partial \Psi_{\mathrm{iso}}}{\partial \bar{I}_a}\bigg|_{\bar{I}_a \to 1} = 2(C_{10} + C_{01}), \tag{16}$$

$$K_0 = \frac{\partial^2 \Psi_{\mathrm{vol}}}{\partial J^2}\bigg|_{J \to 1} = \frac{2}{D_1}. \tag{17}$$

The compressibility parameter D_1 can be interpreted as a penalty parameter that enforces incompressibility if small values are chosen. The chosen parameters are listed in Table 1. In this study, D_1 of the silicone rubber is very small and hence it is not taken into account during the procedure of the parameter identification.

2.2. FEM model with rough surface geometry

It is our goal in this study to quantify the surface roughness effects influencing the force–displacement curve obtained from nanoindentation simulations. Hence, a numerical model of a potential real experimental setup, in which such effects play a significant role, is considered. The modelled situation is the nanoindentation with a Berkovich indenter of two soft polymer films: PDMS and silicone rubber. The indentation depth is limited to 50 nm in order to remove the influence of the hard substrates. It is found by the AFM scanning that the most commonly used three-sided Berkovich indenters are not perfectly sharp but have a tip radius in the order of 100 nm. Therefore, a spherical indenter with a radius of 100 nm is chosen to take the realistic geometry of the indenter tip into account. As explained in Section 2.1, the indented polymers PDMS and silicone rubber are assumed to be isotropic and hyperelastic. Generally speaking, a three dimensional model is necessary to represent the inhomogeneous property of the realistic surface topography. However, the computing time occupies a large part in the inverse method and is, as a consequence, a key problem of the method. This often results in a trade-off between the computing cost and the quality of the numerical model. For instance, a 2D plane model or an axisymmetric model is used most commonly to save the computing cost. In this study, the numerical nanoindentation simulation is modelled by using the finite element code, e.g. ABAQUS® 6.10. A plane strain modelling assumption is preferred, because the commonly real surface topography has a lack of axisymmetry and the position of the indenter can be set randomly on the rough surface in the plane strain model. The indenter can be assumed to be a rigid body compared to the soft polymers. We define the indenter as an analytical rigid surface in such a way that the indenter geometry can be modelled exactly with a smooth curve. The geometrical size of the polymer sample is 2 μm $\times$ 2 μm, which is sufficiently large to obtain a homogeneous stress distribution at the bottom and on the side boundaries of the model. The modelling of the surface roughness is explained in details in Section 4. Concerning the irregular geometry of the rough surface topography, 2D finite element meshes of 6 nodes triangular elements with quadratic shape function are used. For each studied configuration, the mesh convergence is checked by using more than 150,000 degrees of freedom. It shows that a refined mesh, consisting at least of 30,000 degrees of freedom, can give converged results. To account for the localised deformation of the layer, it is essential that the density of nodes under the indenter tip is high enough. The rigid indenter is fixed in the horizontal direction and a vertical displacement is applied on to its reference point. The bottom nodes of the mesh are fixed. In the present work, the deformation of the

specimen during the nanoindentation is restricted to a small deformation regime. The maximum displacement is limited to only 2.5% of the layer thickness. Therefore, the influence of the substrate and the friction between the indenter and the layer can be neglected according to [13].

3. Parameter identification

In the present study, the virtual experiments which are performed by using the FEM simulation with the chosen material models replace the real nanoindentation test for the following reasons: On the one hand, it is difficult to generate different types of surface roughness and to separate its effects from other error contributions in real-world experiments. On the other hand, in the case of virtual experiments, it is possible to investigate how accurate the model parameters can be determined from the parameter re-identification routine. In this process, the resulting force–displacement curve is considered as virtual experimental data, which is used instead of real experimental measurements to identify the chosen parameters again. The parameter re-identification strategy is performed in MATLAB® combined with the nanoindentation boundary value problem which is solved by using the finite element analysis with ABAQUS®. From the mathematical point of view such a process represents a numerical optimisation problem minimising the error between the experimental and the computed force–displacement curve with respect to the model parameters, details are described in e.g. [42]. In general, the vector of material parameters $\boldsymbol{\kappa}$ has to be modified to minimise the distance $f(\boldsymbol{\kappa})$ between the virtual experimental data and the prediction of the numerical model. $f(\boldsymbol{\kappa})$ is the so-called objective function of the least squares type. Mathematically this can be formulated as follows: Find $\boldsymbol{\kappa}$ so that

$$f(\boldsymbol{\kappa}) := \frac{\|\mathbf{F}^{num} - \mathbf{F}^{exp}\|}{\|\mathbf{F}^{exp}\|} \longrightarrow \min f(\boldsymbol{\kappa}). \tag{18}$$

Herein

$$\mathbf{F}^{\exp} = [F_{d1}^{\exp}, F_{d2}^{\exp}, F_{d3}^{\exp}, \ldots]^T, \tag{19}$$

is the virtual experimental data, i.e. the vector of reaction force obtained at each displacement increment. The force vectors obtained for the models with an arbitrary set of material parameters are called

$$\mathbf{F}^{num} = [F_{d1}^{num}, F_{d2}^{num}, F_{d3}^{num}, \ldots]^T. \tag{20}$$

The choice of the optimisation-based method for minimising an objective function is a topic of interest. It is generally advised to use globally convergent optimisation algorithms whenever possible. These algorithms are simulated annealing or genetic algorithms, such as evolutionary algorithms, or deterministic algorithms like the Simplex method. The gradient-based algorithm is full of troublesome gradient calculation and the further drawback of local convergence. Genetic or evolutionary algorithms are globally convergent and are the only useful choice in multi-objective optimisation. Therefore, the evolution strategy is applied in order to find the optimal vector of the material parameters and in order to minimise the objective function. This strategy is based on the principle of the biological evolution and can work with a Genetic Algorithm, which has been implemented in MATLAB® optimisation tool box, for details please see [43,44]. At the beginning, a number λ of different parameter vectors are selected as population individuals $\boldsymbol{\kappa}_{\lambda}^{(g)}$ at generation $g = 0$ in a physically sound range based on a starting vector $\boldsymbol{\kappa}_0$. The selection operator then produces the parent population $\boldsymbol{\kappa}_{\mu}^{(g)}$ of the next generation $g = g + 1$ through a deterministic procedure, which chooses the μ best individuals from the set of λ individuals $(\boldsymbol{\kappa}_1, \ldots, \boldsymbol{\kappa}_{\lambda})$ according to their objective function value $f(\boldsymbol{\kappa})$.

$$(\boldsymbol{\kappa}_{1;\lambda}, \boldsymbol{\kappa}_{2;\lambda}, \ldots, \boldsymbol{\kappa}_{\mu;\lambda}) := Selection_{f(\mu)}(\boldsymbol{\kappa}_1, \ldots, \boldsymbol{\kappa}_{\lambda}), \quad \lambda \geq \mu \tag{21}$$

$$f_{1;\lambda} \leq f_{2;\lambda} \leq \cdots \leq f_{m;\lambda} \leq \cdots \leq f_{\lambda;\lambda} \tag{22}$$

The symbol $(\cdot)_{m;\lambda}$ here stands for the individual with the mth best objective function values. The descendants $\boldsymbol{\kappa}_{\lambda}^{(g)}$ are generated by recombination and by random mutations of the selected parents. In details, a crossover recombination operator randomly selects genetic information from two parents as the vector entry of the descendant. Single parents generate descendants by mutation, in which a stochastic vector $\boldsymbol{\Delta\sigma}$ is added to them. Mutation is the most important ingredient for the evolution strategy, the choice of $\boldsymbol{\Delta\sigma}$ closely links to the convergence behaviour of the method. In order to make the algorithm efficient, it is suggested that $\boldsymbol{\Delta\sigma}$ should be modified during the minimum search. Besides the mutation and the recombination procedures, the parents with the best fitness are guaranteed to survive in the generation $g = g + 1$ as elite individuals.

4. Results of simulation and parameter identification

To the best knowledge of the authors, in most of the papers, the O&P method is used as the post-treatment method of nanoindentation with surface roughness effects. In this method, the hardness and the elastic modulus can be computed based on the unloading segment of the load–displacement curve and the contact area. However, this method has limitations with regard to quantify the surface roughness effects. Firstly, the influence of the surface roughness is evaluated only on the obtained hardness and elastic modulus. Besides, for some shallow indentations, the loading segment of the

Table 2
The identified parameters and the deviation in % compared with the chosen values.

Materials	Chosen models	Identified parameters			Evaluated
			C_{10}	D_1/C_{01}	μ_0
PDMS	Neo-Hookean	Values	0.6614 MPa	0.2543 MPa	1.3228 MPa
		Deviation	0.06%	0.27%	0.09%
Silicone Rubber	Mooney–Rivlin	Values	0.1001 MPa	0.0495 MPa	0.2992 MPa
		Deviation	9.82%	26.92%	0.27%

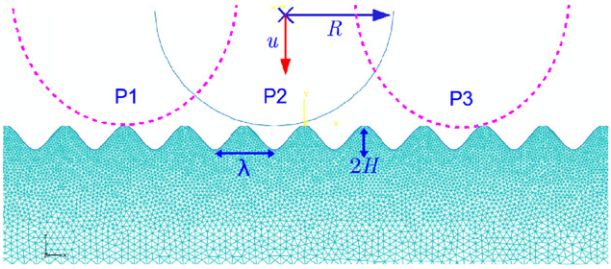

Fig. 1. The mesh configuration of the one-level protuberance-on-protuberance profile.

load–displacement curve, containing a significant influence of the surface roughness, is not used in the O&P method. Furthermore, the contact area is evaluated in this method by using the contact depth and the geometry of the indenter. A polynomial contact area function of contact depth is given by Oliver and Pharr based on the assumption of a perfectly smooth contact interface. Except the pile-up and sink-in phenomena, the surface roughness has a strong influence on the real contact area. However, it is difficult to evaluate accurately the real contact area of a rough contact interface in a real life experiment. In a numerical simulation the contact area can be obtained explicitly, but it is strongly dependent on the mesh size close to the indenter. Therefore, in the present study, the inverse method is used to quantify the influence of the surface roughness. On the one side, it is possible to evaluate the influence of the surface roughness on the identification of all model parameters not only on the hardness and the elastic modulus. On the other side, all segments of the load–displacement curve can be taken into account and the troublesome evaluation of the real contact area can be avoided.

4.1. Indentation of a flat surface

First of all, the nanoindentation of a perfectly flat surface is considered with special focus on the accuracy of the parameter identification. Moreover, the results can be used as a reference in the following discussion about the influence of the surface roughness. The identified parameters and the deviation compared with the chosen values are listed in Table 2. The parameters C_{10} and D_1 of the neo-Hookean model are exactly identified as can be seen in Table 2. This is not the case for the identified parameters C_{10} and C_{01} of the Mooney–Rivlin model. The identified C_{01} differs from the chosen value about 27%. As it is explained in [8,11], the contribution to the force–displacement results from C_{10} and C_{01} cannot be divided. Such phenomenon is called parameter coupling. It has strong influence on the parameter identification of the polynomial-type hyperelastic model. Concerned with the neo-Hookean model, D_1, not similar to C_{10}, is a compressibility parameter. Therefore, the neo-Hookean model is free of parameter coupling during the identifying procedure. Nevertheless, using the identified parameters according to Eq. (16), the evaluated shear modulus μ_0 is approximately the same as the value chosen in Table 1, i.e. the sum $C_{10} + C_{01}$ is identified correctly.

4.2. Indentation of a surface with regular roughness

The surface roughness effects are investigated numerically based on a phenomenological approach. Firstly a simple representation of the surface is chosen considering only a one-level of protuberance-on-protuberance profile described by a sine function $f(x) = H \sin \frac{2\pi}{\lambda} x$, although this simplest model is only a regular wavy surface. It is the preferred model for us to perform the parametric investigation of the surface roughness effects. Moreover, most man-made surfaces such as those produced by grinding or machining, have a pronounced "lay", which may be modelled to a first approximation by this sinusoidal profile [45]. The parameters of the sinusoidal surface profile as well as the indentation geometric parameters are illustrated in Fig. 1: the wave length λ, the roughness asperity height H, the spherical radius R and the indentation depth u. The whole indented sample surface, not only the part just under the indenter, is represented by the sinusoidal profile. This means that the influence of the interaction between the neighbouring asperities of the real surface roughness is also taken into account. It has been shown experimentally that the influence of the surface roughness is dependent on the asperity shape [19]. A large range of roughness asperity shapes from relatively sharp to smooth geometries is obtained by varying the asperity height $H = [5\ \text{nm} \cdots 50\ \text{nm}]$ and by varying the wave length $\lambda = [5\ \text{nm} \cdots 200\ \text{nm}]$.

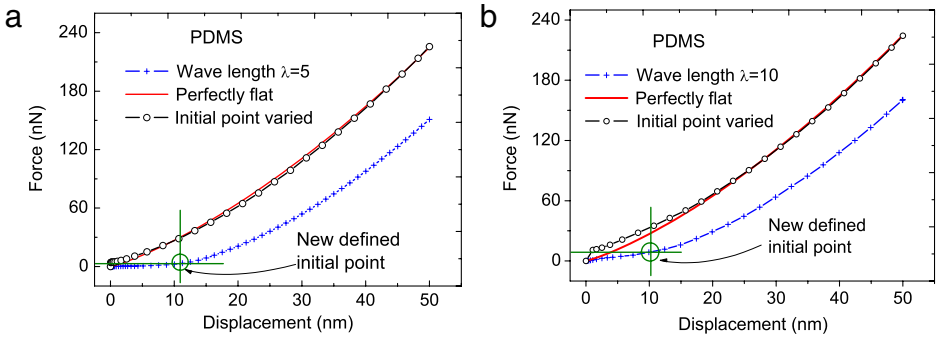

Fig. 2. The force–displacement data obtained from indentation on flat surface and regular rough surface of PDMS, with a varying wave length: (a) $\lambda = 5$ nm; (b) $\lambda = 10$ nm. **Remark**: The new initial point of the force–displacement data is defined by a threshold of the measured reaction force. This is the usual way to define the initial contact of indents and surface in real experiments.

Table 3
The identified parameters and their deviation compared with the chosen values listed in parentheses: indentation on a regular surface roughness.

Experimental data	Identified parameters		Evaluated
	C_{10}	D_1/C_{01}	μ_0
PDMS			
Wave length $\lambda = 5$	0.2941 (−55.57%)	0.1001 (−60.78%)	0.5882 (−55.57%)
Initial point varied $\lambda = 5$	0.6288 (−5.02%)	0.2182 (−14.43%)	1.258 (−5.02%)
$\lambda = 100$_P1	0.6908 (+4.35%)	0.9818 (+285.02%)	1.382 (+4.35%)
Average_P2+P3 $\lambda = 100$	0.6740 (+1.81%)	0.2476 (−2.90%)	1.348 (+1.81%)
Silicone Rubber			
$H = 5$_P2	0.1017 (−8.38%)	0.0429 (+10.00%)	0.2889 (−3.60%)
$H = 20$_P2	0.0605 (−45.50%)	0.0769 (+97.18%)	0.2748 (−8.40%)
$H = 50$_P2	0.0318 (−71.32%)	0.0265 (−32.05%)	0.1167 (−61.11%)

At first, it is focused on varying the wave length λ from 5 nm to 200 nm and keeping the asperity height fixed at 20 nm for each roughness configuration. The results show that the influence of the surface roughness depends strongly on the wave length. This dependence is the same for the PDMS and for the silicone rubber. However, the surface roughness can have a twofold effect resulting in either higher or lower contact stiffness. This twofold effect depends on the indentation position once the wave length increases to be comparable to the indenter radius. As shown in Fig. 1, the three indentation positions are noted as P1, P2 and P3, denoting the indentation performed on the top, in a roughness valley and between the valley and the top respectively. The force–displacement data of the PDMS with a very narrow wave length of 5 nm to 10 nm are shown in Fig. 2. In the two cases, the low ratio λ/H leads to a very sharp asperity. The surface roughness has an effect resulting in much lower contact stiffness especially at the very beginning of the indentation. A physically sound reason can be the response of the extremely sharp asperity, which decreases the material stiffness. The criteria to remove the surface roughness effect suggested in [20] by using a sufficiently large spherical indenter, has no use in this case. Nevertheless, the surface roughness effect on the force–displacement curve can be removed if a new initial indentation point is defined as shown in Fig. 2. The initial contact point between indenter and surface can be re-defined to throw off the contact part in which the contact stiffness is nearly zero. In practice, there are several points nearly zero. In this case, the chosen of the new initial contact point is experience dependent or a method like zero point correction [10] can be applied. The identified parameters are listed in Table 3, it can be seen that this criterion is useful to remove the surface roughness effects if the inverse method is applied based on the force–displacement data only. The surface roughness effect decreases with an increasing wave length up to 50 nm. The roughness effect depends on the indentation position if the wave length is larger than 50 nm as shown in Fig. 3. It can be seen explicitly that the surface roughness results in higher contact stiffness if the indentation is placed in a roughness valley and a decreasing stiffness if an asperity top is indented. This discovery has the same results as documented in [19]. In the real life experiments it is difficult to choose the indentation position neither in the valley or on the top. Therefore, it is reasonable to perform a sufficiently large number of indentations with arbitrary positions from the point of view of statistics. It is a good choice to take the mean value of the data with a reasonable discreteness in order to decrease the surface roughness effect. For instance, we can take the mean values "$\lambda = 100$_P2 & P3ïn Fig. 3(a) and "$\lambda = 200$_P1 & P3ïn Fig. 3(b) as the measured force–displacement data. We can also find similar conclusions in experimental as well as numerical investigations on hard metals in [26,27,30].

The dependence of the surface roughness effect on the asperity height is investigated in the second step. In this case, the wave length is firstly fixed to 50 nm while the asperity height varies in a physically sound range from 5 nm to 50 nm. As the surface roughness has the same influence for the two investigated materials, only the results of the silicone are shown in Fig. 4 in this time. The surface roughness has an effect on the force–displacement data depending on the ratio

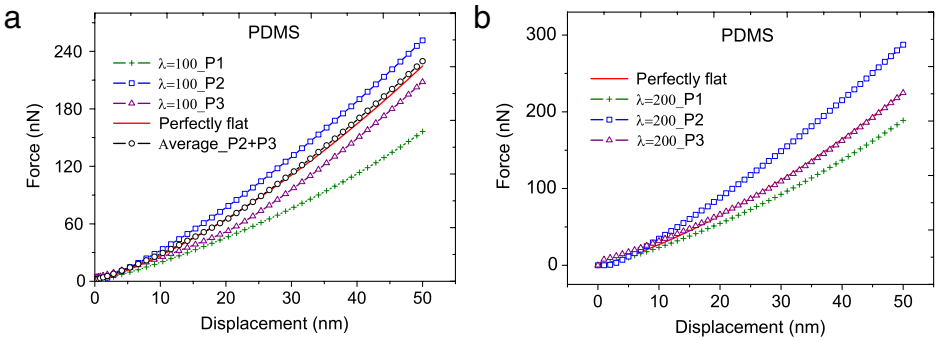

Fig. 3. The force–displacement data obtained from indentation on flat surface and regular rough surface of PDMS, with a varying wave length: (a) $\lambda = 100$ nm; (b) $\lambda = 200$ nm.

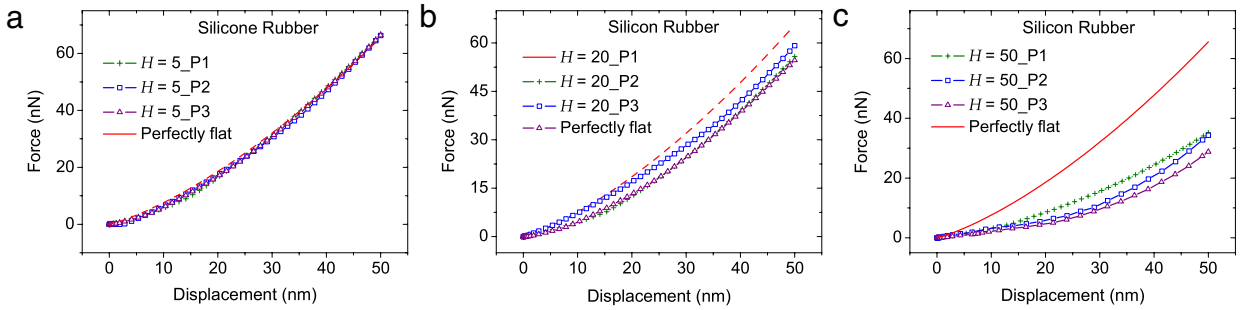

Fig. 4. The force–displacement data obtained from an indentation on a flat surface and a regular rough surface of silicone rubber with varying asperity height: (a) $H = 5$ nm; (b) $H = 20$ nm; (c) $H = 50$ nm.

of the asperity height to the indentation depth H/u. An error contribution of the surface roughness in the inverse method cannot be perceived if H/u is sufficiently small, e. g. 1:10. The indentation result on a perfectly flat surface can still be used to approximate the measuring data indented on rough surface while the ratio H/u is below 1:3. A similar finding was also obtained by Donnelly et al. [29] in an experimental investigation of the indentation on cancellous bone. Nevertheless, the surface roughness effect results in decreasing contact stiffness of approximately 50% lower if the indentation depth is identical to the asperity height.

Finally, the surface roughness effects are quantified by the parameter identification. The virtual experimental data, namely the force–displacement data shown in Figs. 2–4, represent the indentation results obtained with the regular surface roughness model and with the chosen material parameters. The numerical data are the simulation results of the indentation on a perfectly flat surface with an arbitrary set of material parameters. All of the other geometrical parameters and of the boundary value problems of the virtual experimental setup and the numerical model are identical. The comparison of the identified parameters with the chosen values can be used to quantify the surface roughness effects. The identified parameters and the corresponding deviation are compared with the chosen values as shown in Table 3. The identified parameters C_{10} and D_1 of the neo-Hookean model are about 60% lower than the chosen values due to the effects of surface roughness with a wave length of 5 nm. It is worth to note that C_{10} and D_1 are accurately identified if a new initial point is defined to remove the surface roughness effects. The effects result in a much larger identified D_1 if the experiments are performed on the top of the asperity with a wave length of 100 nm. Nevertheless, if the experimental data is replaced by the mean value of the indentation results on different positions, C_{10} and D_1 are exactly identified for the neo-Hookean model. The two parameters C_{10} and C_{01} of the Mooney–Rivlin model are accurately identified if the surface roughness possesses a low asperity height of 5 nm. The surface roughness with the asperity height of 20 nm leads to deviations of -45.50% and $+97.18\%$ for C_{10} and C_{01} respectively. But the evaluated initial shear modulus μ_0 using the identified parameters has an acceptable deviation from the reference value. The surface roughness effects can be neglected with respect to the results shown in Fig. 4(b) and w. r. t. to the evaluated shear modulus μ_0. The existing parameter coupling is the main reason to cause a big deviation to the identified C_{10} and C_{01}. The surface roughness has an effect on the evaluated μ_0 resulting in a 61.11% lower value.

4.3. Indentation on a realistic surface roughness model

In general the real surface has a roughness containing various wave lengths and asperity heights distributed irregularly if it is scanned by the AFM technique in a nano-scale. The use of a simple regular model like in Section 4.2 may has a limited domain of validity of the numerical simulation and the obtained quantified results. Moreover, in order to minimise

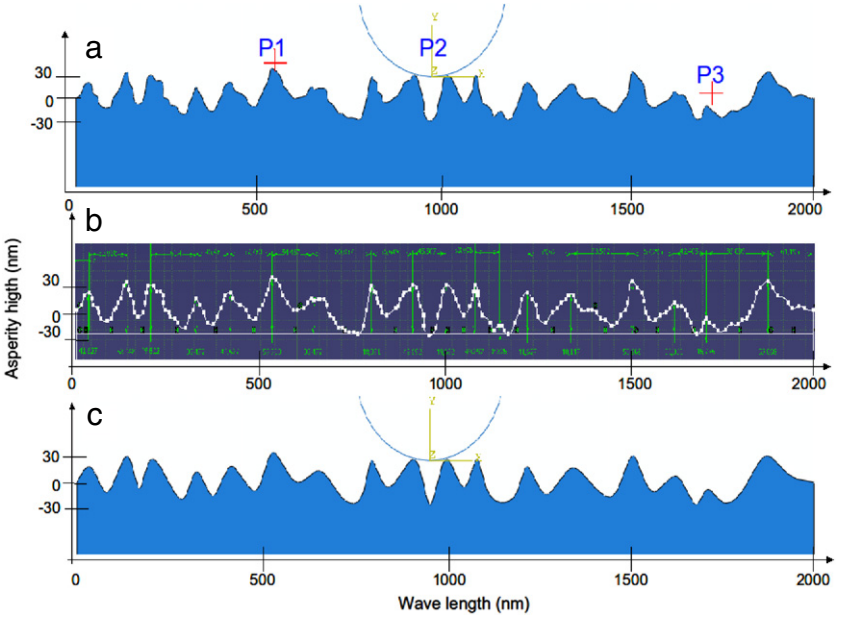

Fig. 5. The surface profile of a more realistic roughness model: (a) FEM geometry model of the realistic rough surface; (b) Measuring the random asperity; (c) Simplifying (a) with a multi-level sinusoidal curve in FEM model.

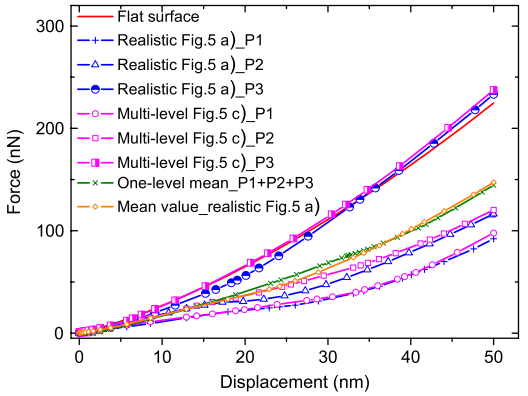

Fig. 6. Direct comparison of the force–displacement data of indentation with different positions on realistic surface roughness, multi-level sinusoidal profile model and one-level simple surface model.

the system errors due to the surface roughness effects, it is also necessary to take a realistic surface roughness model into account. A more realistic surface profile, depicted in Fig. 5(a), is modelled with irregularly various serration. Three typical indentation positions on this topography are considered with an indentation depth of 50 nm after an initial contact. A multi-level protuberance-on-protuberance sine profile is considered to simplify this serration surface model. It is measured the asperity height and the wave length of the realistic roughness by dividing the serration form into several continuous pieces, as shown in Fig. 5(b). The transformation can be performed with a CAD program and is then input into ABAQUS®. A simplified realistic surface model is plotted in Fig. 5(c). It is described by using multi-level sinusoidal functions $f_i(x) = H_i \sin\left(\frac{2\pi}{\lambda_i} x + \theta_i\right)$, with different wave length λ_i, amplitudes H_i and phase shifts θ_i. These parameters can be obtained by a Fourier transformation. Three indentations with different positions, the same as shown in Fig. 5(a), are made on this surface. The force–displacement results of the two realistic models are at first compared directly in Fig. 6. Firstly, the force–displacement data of the realistic model and the multi-level sinusoidal profile model depends strongly on the indentation position. The response to the deformation of the stochastic local topography plays an important role in the whole indentation results. Secondly, comparing the data of the same indentation position, it is found that the multi-level sinusoidal model can be used to predict the realistic surface roughness effects. The deformed configurations at the maximum displacement indented on positions P1, P2, P3 are shown in Fig. 7. They are obtained from the realistic surface roughness model as shown in Fig. 5(a) and the multi-level sinusoidal profile model as shown Fig. 5(b), respectively. These deformed configurations are able to illustrate the force–displacement results explained above. The indentation data of the

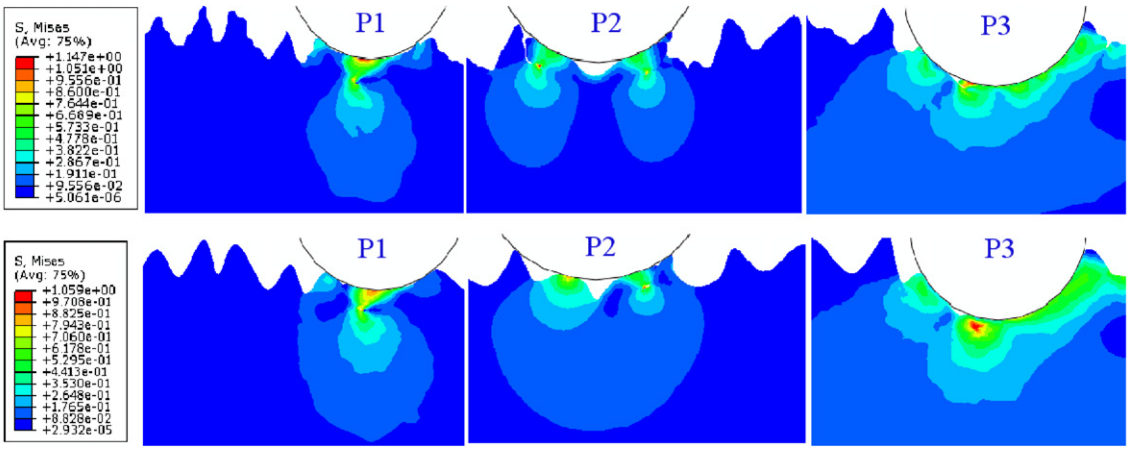

Fig. 7. The deformed configurations at the maximum displacement indented on positions P1, P2, P3 obtained from the realistic surface roughness model as shown in Fig. 5(a) (above) and the multi-level sinusoidal profile model as shown Fig. 5(b) (below).

Table 4
The identified parameters and its deviation compared with the chosen values listed in parentheses: indentation on a realistic surface roughness model.

Numerical model	Identified parameters		Evaluated
	C_{10}	D_1/C_{01}	μ_0
PDMS			
Flat surface model	0.4946 (−25.29%)	0.7494 (+193.88%)	0.9892 (−25.29%)
One-level sine profile	0.7031 (+6.21%)	0.4366 (+71.72%)	1.4062 (+6.21%)
Silicone Rubber			
Flat surface model	0.0538 (−51.53%)	0.0279 (−28.46%)	0.1634 (−45.53%)
One-level sine profile	0.0944 (−14.95%)	0.0489 (+25.38%)	0.2866 (−4.47%)

perfectly flat surface is also plotted in Fig. 6. It is worth to mention that the response of indentation on the position P3 is able to predict well the indentation behaviour of the perfectly flat surface. The local topography of the position P3 is distributed with a large wave length as well as low asperities of either a negative or a positive skew. This type of position is a good choice to decrease the error contribution due to surface roughness in a realistic experimental setup. There are many different roughness parameters in use, but R_a, called arithmetic average roughness, is the most commonly used parameter. The R_a of the realistic surface roughness model in Fig. 5 can be estimated from $R_a = 1/n \sum_{i=1}^{n} |y_i|$, y_i denote the wave length λ_i, the asperity height H_i and the phase shifts θ_i, respectively. A numerical model with the roughness of a one-level sine function of R_a is applied to predict the statistics indentation force–displacement data with effects of realistic surface roughness. It can be seen in Fig. 6 that the numerical simulation with this one-level roughness model is able to predict the statistical mean value of the force–displacement data of indentation with the effects of a realistic surface roughness.

In the second step, the model parameters of the two polymers are identified. The statistics mean force–displacement data, obtained from the realistic model Fig. 5(a) with the chosen parameters, serves as the experimental data. The FEM models with a perfectly flat surface and a one-level sine curve surface profile are used to predict the numerical data with the arbitrary set of material parameters. The identified parameters and the corresponding deviations are listed in Table 4. It shows explicitly that the identified parameters have large deviations compared with the chosen values if a numerical model with flat surface is used. The surface roughness effects which are not taken into account in the numerical model yield much big deviations of the identified parameters. Nevertheless, the parameters are accurately identified if the surface roughness described by a simple one-level sine function of the arithmetic average roughness R_a is taken into account. From this point of view, the realistic surface roughness can be modelled by using a simple one-level sine function in the process of parameter identification.

5. Conclusions and discussion

In this paper, the characterisation of two often used soft hyperelastic polymers, PDMS and silicone rubber, is investigated by nanoindentation taking into account effects of the surface roughness. The inverse method is applied to quantify the influence of the variable topography on the identified values of the model parameters.

At first, the parametric investigation of the surface roughness effects is performed by indentation on a regular surface roughness described by a one-level sine function. The surface roughness effects strongly depend on the roughness shape, namely the wave length λ and the asperity height H. The indentation on a very sharp asperity with a low ratio λ/H leads

to a decreased contact stiffness compared to a flat surface especially at the initial indentation. The identified values of the parameters C_{10} and D_1 of the neo-Hookean model are about 60% lower than the chosen values due to the effects of surface roughness with a wave length of 5 nm. Nevertheless, the surface roughness effect on the force–displacement curve can be avoided if a new initial indentation point is defined by a certain threshold of the resulting contact force. In this case, the re-identified parameters have an acceptable deviation from the chosen values. The surface roughness effect results in higher contact stiffness with an indentation in the roughness valley and a lower one with the indentation on an asperity top, if the wave length is larger than 50 nm. If the experimental data is replaced by the mean value of the indentation results on different positions, C_{10} and D_1 are exactly identified compared with the chosen values. To take the mean data of the sufficiently large number of indentations is a good choice to decrease the error contribution of surface roughness to the identification process. The surface roughness effect on the force-dependent data also depends on the ratio H/u. The indentation model with a perfectly flat surface can still be used to approximate the force–displacement data indented on a rough surface if H/u is below 1:3. The parameter coupling exists if the two parameters C_{10} and C_{01} of the Mooney–Rivlin model are identified using experimental data with surface roughness effects. In this case, the initial shear modulus μ_0 evaluated from the identified parameters C_{10} and C_{01} is a suitable choice to quantify the surface roughness effects.

In a second step, a more realistic surface roughness profile is modelled with irregularly various serrations. It is verified that a multi-level protuberance-on-protuberance sine profile can be used to simplify this serration surface model. Furthermore, this realistic surface model is simplified by using a one-level sinusoidal profile model described with the arithmetic average roughness R_a. The identified parameters of the two models have large deviations compared with the chosen values because of the surface roughness effects, which are considered in the numerical model. Nevertheless, the parameters are accurately identified if a surface roughness described by a simple one-level sine function is taken into account. In this case, the statistic parameters of the realistic surface roughness, e. g. the arithmetic average roughness R_a, should be used to describe the simple roughness profile.

The investigated results and findings in this study can be used in the polishing of the sample in real experiments and in the numerical simulation if the inverse method is applied to quantify the model parameters. It is one choice to model the realistic surface roughness in order to minimise the systematic error due to surface roughness between experimental setup and the numerical model. The surface scanning from AFM may help us to get the true local roughness shape of the sample surface. Like we did in this study, a multi-level or a one-level sinusoidal profile model described with statistics roughness parameters can be used in the numerical simulation. Moreover, the often used fast Fourier transform (FFT) in the treatment of signals can be considered to deal with the random realistic roughness. Concerned with the inhomogeneous property of the realistic surface topography, a 3D model is necessary to represent the real shape in the numerical simulation. However, the huge computational cost often results in a trade-off between the computing cost and the quality of the numerical model. In this case, a second choice can be considered to solve this problem. The idea is based on quantifying the surface roughness effects on the force–displacement data. The realistic surface roughness can be characterised by some statistics parameters: the arithmetic average roughness R_a, root mean squared roughness *RMS*, maximum valley depth R_v, and maximum peak height R_p. The contributions from the surface roughness to the force–displacement data can be quantified as a function of the roughness parameters based on mathematical statistical methods. The calibrated experimental force–displacement data, using these quantified functions, could be considered as experimental data without the surface roughness effects. Therefore, it is reasonable to use a 2D numerical model with flat surface if the inverse method is applied. A further investigation on the topic of surface roughness effects in nanoindentation based on this idea is the work in hand and the results will be documented in an upcoming paper.

Acknowledgements

The authors are grateful to the DFG (German Science Foundation—Deutsche Forschungsgemeinschaft) for financial support through the grant number Di 430/14-1&2. The work of the student research assistant Martin Müller, Univ. Saarland, is appreciated.

References

[1] W.C. Oliver, G.M. Pharr, An improved technique for determining hardness and elastic modulus using load and displacement sensing indentation experiments, J. Mater. Res. 7 (1992) 1564–1583.
[2] W.C. Oliver, G.M. Pharr, Measurement of hardness and elastic modulus by instrumented indentation: advance in understanding and refinements to methodology, J. Mater. Res. 19 (2004) 3–20.
[3] N. Huber, W.D. Nix, H. Gao, Identification of elastic–plastic material parameters from pyramidal indentation of thin films, Proc. R. Soc. Lond. Ser. A 458 (2002) 1593–1620.
[4] S. Guessasma, M. Sehaki, D. Lourdin, A. Bourmaud, Viscoelasticity properties of biopolymer composite material determined using finite element calculation and nanoindentation, Comp. Mat. Science 44 (2008) 371–377.
[5] S. Hartmann, J. Gibmeier, B. Scholtes, Experiments and material parameter identification using finite elements. uniaxial tests and validation using instrumented indentation tests, Exp. Mech. 46 (2006) 5–18.
[6] N. Huber, E. Tyulyukovskiy, A new loading history for identification of viscoplastic properties by spherical indentation, J. Mater. Res. 19 (2004) 101–113.
[7] D. Klötzer, C. Ullner, E. Tyulyukovskiy, N. Huber, Identification of viscoplastic material parameters from spherical indentation data. part II: experimental validation of the method, J. Mater. Res. 21 (2006) 677–684.
[8] G. Rauchs, J. Bardon, D. Georges, Identification of the material parameters of a viscous hyperelastic constitutive law from spherical indentation tests of rubber and validation by tensile tests, Mech. Mater. 42 (2010) 961–973.

[9] G. Rauchs, J. Bardon, Identification of elasto-viscoplastic material parameters by indentation testing and combined finite element modelling and numerical optimization, Finite Elem. Anal. Des. 47 (2011) 653–667.
[10] E. Tyulyukovskiy, N. Huber, Identification of viscoplastic material parameters from spherical indentation data. part i: neural networks, J. Mater. Res. 21 (2006) 664–676.
[11] Z. Chen, S. Diebels, Nanoindentation of hyperelastic polymer layers at finite deformation and parameter re-identification, Arch. Appl. Mech. (2011) 1–16. http://dx.doi.org/10.1007/s00419-012-0613-9.
[12] Z. Chen, S. Diebels, Numerical investigation of nanoindentation of viscoelastic polymer layers and parameters re-identification, PAMM Proc. Appl. Math. Mech. 11 (2011) 765–766.
[13] Z. Chen, S. Diebels, J. Schmitt, Frictional nanoindentation of hyperelastic polymer layers: A numerical study, in: Proceedings of the 3rd ECCOMAS Thematic Conference on the Mechanical Response of Composites, 2011, pp. 229–236.
[14] G. Bolzon, G. Maier, M. Panico, Material model calibration by indentation, imprint mapping and inverse analysis, Int. J. Solid Struct. 41 (2004) 2957–2975.
[15] M. Mata, J. Alcalá, The role of friction on sharp indentation, J. Mech. Phys. Solids 455 (2004) 145–165.
[16] E. Tyulyukovskiy, N. Huber, Neural networks for tip correction of spherical indentation curves from bulk metals and thin metal films, J. Mech. Phys. Solids 55 (2007) 391–418.
[17] M.S. Bobji, S.K. Biswas, Deconvolution of hardness from data obtained from nanoindentation of rough surfaces, J. Mater. Res. 14 (1999) 2259–2268.
[18] M.S. Bobji, K. Shivakumar, H. Alehossein, V. Venkateshwarlu, S.K. Biswas, Influence of surface roughness on the scatter in hardness measurements—a numerical study, Int. J. Rock Mech. Min. Sci. Geomech. Abstr 36 (1999) 399–404.
[19] P. Berke, F.E. Houdaigui, T.J. Massart, Coupled friction and roughness surface effects in shallow spherical nanoindentation, Wear (2010).
[20] W.G. Jiang, J.J. Su, X.Q. Feng, Effect of surface roughness on nanoindentation test of thin films, Eng. Fract. Mech. 75 (2008) 4965–4972.
[21] A.K.N. Kumar, M.D. Kannan, S. Jayakumar, K.S. Rajam, V.S. Raju, Investigations on the mechanical behaviour of rough surfaces of tini thin films by nanoindentation studies, Surf. Coat. Technol. 201 (2006) 3253–3259.
[22] J.Y. Kim, S.K. Kang, J.J. Lee, J. Jang, Y.H. Lee, D. Kwon, Influence of surfaceroughness on indentation size effect, Acta Mater 55 (2007) 3555–3562.
[23] J.Y. Kim, J.J. Lee, Y.H. Lee, J. Jang, D. Kwon, Surface roughness effect in instrumented indentation: a simple contact depth model and its verification, Acta Mater 55 (2007) 3555–3562.
[24] M. Qasmi, P. Delobelle, Influence of the average roughness rms on the precision of the young's modulus and hardness determination using nanoindentation technique with a berkovich indenter, Surf. Coat. Technol. 201 (2006) 1191–1199.
[25] S.W. Wai, G.M. Spinks, H.R. Brown, M. Swain, Surface roughness: its implications and inference with regards to ultra microindentation measurements of polymer mechanical properties, Polym. Test 23 (2004) 501–507.
[26] C. Walter, T. Antretter, R. Daniel, C. Mitterer, Finite element simulation of the effect of surface roughness on nanoindentation of thin films with spherical indenter, Surf. Coat. Technol. 202 (2007) 1103–1107.
[27] C. Walter, C. Mitterer, 3d and 2d finite element simulation of the effect of surface roughness in nanoindentation of hard coatings, Surf. Coat. Technol. 203 (2008) 3286–3290.
[28] M. Miller, C. Bobko, M. Vandamme, F.J. Ulm, Surface roughness criteria for cement paste nanoindentation, Cement and Concrete Research 38 (2008) 467–476.
[29] E. Donnelly, S.P. Baker, A.L. Boskey, M.C.H. van der Meulen, J. Biomed, Effects of surface roughness and maximum load on the mechanical properties of cancellous bone measured by nanoindentation, J. Biomed. Mater. Res. - Part A 77 (2006) 426–435.
[30] K.D. Bouzakis, N. Michailidis, S. Hadjiyiannis, G. Skordaris, G. Erkens, The effect of specimen roughness and indenter tip geometry on the determination accuracy of thin hard coatings stress–strain laws by nanoindentation, Mater. Charact. 49 (2003) 149–156.
[31] T.H. Fang, W.J. Chang, C.M. Lin, Nanoindentation characterization of zno thin films, Mater. Sci. Eng. A 452–453 (2007) 715–720.
[32] G.B. de Souza, C.E. Foerster, S.L.R. da Silva, F.C. Serbena, C.M. Lepienski, C.A. dos Santos, Hardness and elastic modulus of ion-nitrided titanium obtained by nanoindentation, Surf. Coat. Technol. 191 (2006) 76–82.
[33] G. Rauchs, Optimization-based material parameter identification in indentation testing for finite strain elasto-plasticity, ZAMM Z. Angew. Math. Mech. 86 (2006) 539–562.
[34] J. Deuschle, Mechanics of soft polymers indentation, Doctoral Thesis, Universität Stuttgart, 2008.
[35] M. Johlitz, S. Diebels, Characterisation of a polymer using biaxial tension tests. part i: hyperelasticity, Arch. Appl. Mech. (2010) 1–17. http://dx.doi.org/10.1007/s00419-010-0480-1.
[36] G.A. Holzapfel, Nonlinear Solid Mechanics: A Continuum Approach for Engineering, Lohn Wiley & Sons Ltd, England, 2001.
[37] W. Ehlers, G. Eipper, The simple tension problem at large volumetric strains computed from finite hyperelastic material laws, Acta Mech. 130 (1998) 17–27.
[38] R.W. Penn, Volume changes accompanying the extension of rubber, Trans. Soc. Rheol 14 (1970) 509–517.
[39] S. Hartmann, P. Neff, Polyconvexity of generalized polynomial-type hyperelastic strain energy functions for near-incompressibility, Int. J. Solids Struct. 40 (2003) 2767–2791.
[40] J.C. Simo, R.L. Taylor, Penalty function formulations for incompressible nonlinear elastostatics, Comput. Methods Appl. Mech. Eng. 35 (1982) 107–118.
[41] S. Doll, K. Schweizerhof, On the development of volumetric strain energy functions, J. Appl. Mech. Trans. ASME 67 (2000) 17–21.
[42] J. Nocedal, S.J. Wright, Numerical Optimization, Springer-Verlag, New York, LLC. United States of America, 1999.
[43] H.P. Schwefel, Evolution and Optimum Seeking, Wiley, New York, 1995.
[44] H.G. Beyer, The Theory of Evolution Strategy, Springer, 2001.
[45] K.L. Johnson, Contact Mechanics, Cambridge University Press, 1985.